RMetS
Royal Meteorological Society

Cascades, backscatter and conservation in numerical models of two-dimensional turbulence

John Thuburn,[a]* James Kent[a,b] and Nigel Wood[c]

[a]*College of Engineering, Mathematics and Physical Sciences, University of Exeter, UK*
[b]*Department of Atmospheric, Oceanic and Space Sciences, University of Michigan, Ann Arbor, MI, USA*
[c]*Met Office, FitzRoy Road, Exeter UK*

*Correspondence to: J. Thuburn, College of Engineering, Mathematics and Physical Sciences, University of Exeter, Harrison Building, North Park Road, Exeter EX4 4QF, UK. E-mail: j.thuburn@exeter.ac.uk

The equations governing atmospheric flow imply transfers of energy and potential enstrophy between scales. Accurate simulation of turbulent flow requires that numerical models, which have finite resolution and truncation errors, adequately capture these interscale transfers, particularly between resolved and unresolved scales. It is therefore important to understand how accurately these transfers are modelled in the presence of scale-selective dissipation or other forms of subgrid model. Here, the energy and enstrophy cascades in numerical models of two-dimensional turbulence are investigated using the barotropic vorticity equation.

Energy and enstrophy transfers in spectral space due to truncated scales are calculated for a high-resolution reference solution and for several explicit and implicit subgrid models at coarser resolution. The reference solution shows that enstrophy and energy are removed from scales very close to the truncation scale and energy is transferred (backscattered) into the large scales. Some subgrid models are able to capture the removal of enstrophy from small scales, though none are scale-selective enough; however, none are able to capture accurately the energy backscatter.

We propose a scheme that perturbs the vorticity field at each time step by the addition of a particular vorticity pattern derived by filtering the predicted vorticity field. Although originally conceived as a parametrization of energy backscatter, this scheme is best interpreted as an energy 'fixer' that attempts to repair the damage to the energy spectrum caused by numerical truncation error and an imperfect subgrid model. The proposed scheme improves the energy and enstrophy behaviour of the solution and, in most cases, slightly reduces the root mean square vorticity errors.

Key Words: backscatter; cascade
Received 30 October 2012; Revised 4 February 2013; Accepted 28 March 2013; Published online in Wiley Online Library 19 June 2013

1. Introduction

The adiabatic frictionless governing equations of atmosphere and ocean dynamics conserve both energy and potential enstrophy. However, the nonlinearity of the governing equations leads to systematic transfers between scales and therefore transfers between scales that are resolvable and those that are unresolvable for any given finite-resolution numerical model. Failure to model these transfers correctly could lead to numerical solutions that are excessively active and noisy or excessively damped at certain scales. It is therefore important to determine how well these interscale transfers are handled in weather forecast and climate models, and to develop improved representations of them. For quasi-geostrophic turbulence, energy is transferred mainly upscale and potential enstrophy is transferred mainly downscale (e.g. see Salmon, 1998). This means that numerical methods that can dissipate potential enstrophy while conserving energy are desirable for atmospheric models, at least in those regions and on those scales for which quasi-geostrophic dynamics are qualitatively correct.

Typically in atmospheric models, the numerical representation of energy and potential enstrophy transfers is achieved either by conservative numerics supplemented with some form of explicit scale-selective dissipation or by the use of inherently dissipative numerics such as semi-Lagrangian or non-oscillatory finite volume schemes (such as Lin, 2004). If a numerical model captures the downscale cascade but conserves potential enstrophy, then potential enstrophy will accumulate near the truncation scale leading to a noisy solution. This is known as 'spectral blocking'. Spectral blocking clearly points to the need for models to remove potential enstrophy near the truncation scale. In practice, all models include some form of explicit or implicit scale-selective dissipation (Jablonowski and Williamson, 2011). This dissipation is applied for many reasons, both physical and numerical, one of

which is to remove potential enstrophy and model the cascade to unresolved scales.

However, a side-effect of potential enstrophy dissipation is that energy is dissipated too. For the barotropic vorticity equation (see section 2), removal of enstrophy at wave number $k_{\rm diss}$, say, at a rate $\dot{Z}$ implies that energy is also removed, at a rate $\dot{E} = \dot{Z}/k_{\rm diss}^2$. This energy removal rate must be at least $\dot{Z}/k_{\rm max}^2$, where $k_{\rm max}$ is the maximum resolvable wave number. In practical weather and climate models, energy and enstrophy are removed over a wide range of wave numbers, so the ratio $\dot{E}/\dot{Z}$ is significantly greater than $1/k_{\rm max}^2$. Enstrophy and available energy budgets estimated for the troposphere (Koshyk and Boer, 1994; Thuburn, 2008, and references therein) suggest an enstrophy throughput $\dot{Z}$ of order $10^{-15}\,{\rm s}^{-3}$ and an energy throughput $\dot{E}$ of order $10^{-5}\,{\rm m}^{-2}{\rm s}^{-3}$ associated with nonlinear downscale cascades in the free atmosphere. (A much larger energy sink of order $10^{-4}\,{\rm m}^{-2}{\rm s}^{-3}$ is associated with boundary layer dissipation.) These numbers suggest an estimate for the average dissipation scale: $k_{\rm diss} \sim 10^{-5}\,{\rm m}^{-1}$. There is evidence in the literature (e.g. Shutts, 2005; Bowler *et al.*, 2009), as well as much anecdotal evidence (e.g. WGNE, 2003) that, at current climate resolutions and even resolutions used for ensemble weather prediction, state-of-the-art models dissipate too much energy in the free atmosphere, perhaps an order of magnitude too much. This excessive dissipation can result in insufficient variability and underdispersive ensembles.

One solution to the problem of excessive energy dissipation is the use of energy fixers. These can be in the form of a frictional heating term or an a posteriori fixer to ensure that energy is conserved (Williamson, 2007; see Neale *et al.*, 2010, for an example). These fixers must be designed so that they do not introduce large errors into the solution, for example by adding energy at an inappropriate location (see Williamson *et al.*, 2009, for an example). However, such fixers may still allow the *available energy* associated with the active dynamics to decrease even if they conserve the total energy. An alternative approach, designed to help maintain variability and eddy activity at realistic amplitudes, is to directly increase the kinetic energy of the flow by perturbing the velocity field. This approach is often viewed as modelling the upscale transfer of kinetic energy from unresolved to resolved scales, and so is termed 'backscatter'. Backscatter models have been developed for three-dimensional large eddy simulations (see Mason and Thomson, 1992; Domaradski and Saiki, 1997) to model the upscale energy transfer near boundaries. Backscatter models have also been developed for large-scale atmospheric models (see Bowler *et al.*, 2009; Berner *et al.*, 2009), where energy that has been dissipated is added back to the solution as kinetic energy, usually as random perturbations.

The barotropic vorticity equation is the simplest relevant fluid system in which to study this problem. In this paper we use a high-resolution reference solution of the barotropic vorticity equation to determine the effect of scales smaller than some specified truncation on the spectral tendencies of energy and enstrophy. This provides a quantitative measure of both downscale cascades and backscatter, and their spectral dependence, which we compare with a variety of explicit and implicit subgrid models (section 3). (A similar approach has been proposed very recently by Pietarila Graham and Ringler, 2013, but with the emphasis on spectral energy and enstrophy fluxes rather than tendencies.)

These results are used to inspire the development of a backscatter model or energy fixer for two-dimensional turbulence that will ensure conservation of energy and dissipation of enstrophy (section 4). The idea is not to use random perturbations but to add energy in patterns that are based on the resolved scale structures, with a sound rationale for the spectral distribution of energy sources and sinks. The proposed scheme is tested on the barotropic vorticity equation and shown to give a reduction in vorticity errors in some cases, as well as improvements in total energy and enstrophy (section 5).

2. Governing equations and numerical schemes

The barotropic vorticity equation is given as

$$\frac{\partial \zeta}{\partial t} + \frac{\partial u\zeta}{\partial x} + \frac{\partial v\zeta}{\partial y} = 0, \tag{1}$$

where $\zeta = v_x - u_y$ is the vorticity, and u and v are the velocity components in the x and y directions respectively. The flow is incompressible, $u_x + v_y = 0$, and the vorticity can be inverted to calculate the stream function (ψ) and the velocity components:

$$\nabla^2\psi = \zeta, \tag{2}$$

$$u = -\psi_y, \tag{3}$$

$$v = \psi_x. \tag{4}$$

We consider the problem in a doubly periodic square domain of unit size.

The continuous equations conserve both energy

$$E = -\frac{1}{2}\int \psi\zeta \,{\rm d}x\,{\rm d}y \tag{5}$$

and enstrophy

$$Z = \frac{1}{2}\int \zeta^2 \,{\rm d}x\,{\rm d}y. \tag{6}$$

However, the nonlinear effects of unresolved scales on resolved scales may be non-negligible, and therefore numerical methods must be able to represent these effects. Formally this may be expressed using a filtered form of the governing equations. For the barotropic vorticity equation, the filtered form is

$$\frac{\partial \overline{\zeta}}{\partial t} + \frac{\partial \overline{\overline{u}\overline{\zeta}}}{\partial x} + \frac{\partial \overline{\overline{v}\overline{\zeta}}}{\partial y} = {\rm SG}, \tag{7}$$

where

$${\rm SG} = \frac{\partial}{\partial x}\left(\overline{\overline{u}\overline{\zeta}} - \overline{u\zeta}\right) + \frac{\partial}{\partial y}\left(\overline{\overline{v}\overline{\zeta}} - \overline{v\zeta}\right) \tag{8}$$

is the subgrid term and an overbar represents a filter that removes scales smaller than the model resolution. (Note that other forms of filtered equations are often used.) As energy and enstrophy transfers between the resolved scales and unresolved scales are mediated by the unresolved scales, the representation of these transfers is intimately related to the representation of the subgrid term SG.

Broadly, there are two approaches for representing the subgrid terms in numerical models: explicit subgrid models and implicit subgrid models. Explicit subgrid models construct a mathematical model for SG in terms of the resolved variables, and add this (or a discretization of it) to the right hand side of the discretized equations. The simplest example is a scale-selective hyperdiffusion of the form $K\nabla^{2n}$, where K is a tunable parameter and n an integer, but a range of more sophisticated schemes have been proposed, such as those by Smagorinsky (1963), Sadourny and Basdevant (1985) and Frederiksen and Kepert (2006).

Implicit subgrid models (also known as implicit large-eddy simulation – ILES) use a discretization of the governing equations whose truncation errors are intended to play the role of a subgrid model. This approach often makes use of finite-volume methods and flux limiters. High-order upwind schemes with flux limiters often have truncation errors that take the form of a nonlinear scale-selective dissipation. The strength of this dissipation adapts to the strain rate of the resolved flow and therefore resembles many physically based explicit subgrid models (Grinstein *et al.*, 2007).

ILES has been examined in detail for three-dimensional turbulence (e.g. Margolin and Rider, 2002, 2007; Grinstein *et al.*, 2007) and some success has been claimed, although it appears less successful when upscale effects are important, for example near walls (Brown *et al.*, 2000). The application of ILES to two-dimensional flow was examined by Kent *et al.* (2012), and it was found that several schemes were able to capture the leading order effects of the subgrid term when those effects were dissipative, for example when vorticity filaments were stretched and thinned to the resolution limit. However, none of the schemes was successful when the subgrid term involved upscale effects such as vortex merger or roll-up of thin vorticity filaments: each of the schemes tested dissipated energy.

In this paper we make use of several numerical methods, with both explicit and implicit subgrid models, in our numerical testing. The first is the spectral transform method (see, for example, Durran, 1999) and the second is the Arakawa Jacobian (Arakawa, 1966). Both use a leapfrog time integration scheme with a weak Robert–Asselin time filter (Robert, 1966; Asselin, 1972). Both schemes conserve energy and enstrophy in the absence of forcing and dissipation terms (apart from a very weak dissipation by the time filter), and so are supplemented with explicit ∇^4 or ∇^8 hyperdiffusion terms, handled with a forward time step for stability. Unless otherwise stated, the dissipation coefficient is chosen to make the dissipation time-scale equal to one time unit at the smallest resolved scale. (This choice of dissipation time-scale is justified as follows. In all of the experiments discussed below the eddy turnover time, and hence the enstrophy cascade time-scale, are around one time unit. In order to prevent the build-up of grid scale noise, the dissipation time-scale at the smallest resolved scale must be comparable to the enstrophy cascade time-scale.)

The next scheme is a version of the UTOPIA scheme (Leonard *et al.*, 1993), which is a quasi-third-order upwind flux-form advection scheme. It may be used with a multidimensional flux limiter (Thuburn, 1996) to prevent overshoots and undershoots. The UTOPIA scheme with and without flux limiting has been shown to perform satisfactorily for the barotropic vorticity equation, and to remove enstrophy from small scales, giving an implicit representation of the cascade of enstrophy to unresolved scales (Kent *et al.*, 2012). Its behaviour is expected to be typical of many upwind finite volume schemes.

The final scheme is the anticipated potential vorticity method (APVM) of Sadourny and Basdevant (1985), which conserves energy while dissipating enstrophy. The scheme is derived by writing the Euler equations in vector-invariant form:

$$\frac{\partial u}{\partial t} - \zeta v + \frac{\partial}{\partial x}\left(\frac{1}{2}(u^2+v^2)+P\right) = 0, \tag{9}$$

$$\frac{\partial v}{\partial t} + \zeta u + \frac{\partial}{\partial y}\left(\frac{1}{2}(u^2+v^2)+P\right) = 0, \tag{10}$$

where P is the pressure. The vorticity ζ in the second term of (9) and (10) is replaced by $\zeta - D$ so that the vorticity equation, obtained by taking $\partial/\partial x(10) - \partial/\partial y(9)$, is

$$\frac{\partial \zeta}{\partial t} + \frac{\partial u(\zeta - D)}{\partial x} + \frac{\partial v(\zeta - D)}{\partial y} = 0. \tag{11}$$

Replacing ζ in the advection terms of Eq. (1) by $\zeta - D$, giving Eq. (11), will have no impact on energy conservation in the continuous equations. Consequently, energy will be conserved if an energy-conserving scheme is used for the $\zeta - D$ advection terms in Eq. (11). At the same time, D may be chosen to ensure that enstrophy is dissipated. The two choices of D that will be considered in this paper are

$$D_2 = \theta\left(u\frac{\partial \zeta}{\partial x} + v\frac{\partial \zeta}{\partial y}\right), \tag{12}$$

$$D_4 = -\nabla^2\left[\theta\left(u\frac{\partial \zeta}{\partial x} + v\frac{\partial \zeta}{\partial y}\right)\right], \tag{13}$$

where θ is a tunable parameter (Sadourny and Basdevant, 1985). The second form D_4 involves higher derivatives of ζ and so is expected to provide more scale-selective dissipation of enstrophy. For stability, the D terms are evaluated using a forward time step, while the other terms are evaluated using a leapfrog time step supplemented by a weak Robert–Asselin filter. In the experiments presented below, a spectral method was used to compute the Jacobian terms in the APVM. We have also experimented with using the Arakawa Jacobian, with similar results (not shown).

For the spectral method and the spectral APVM, ψ is calculated from ζ in Eq. (2) exactly using the spectral method. For the other schemes a finite difference discretization of the Laplacian is used. For all results presented below, the time step is given by $\Delta t = 5.0/N$ when running on an $N \times N$ grid; this is comfortably within the stability limit in all cases.

Several of these schemes were tested in Kent *et al.*(2012) and were shown to dissipate both enstrophy and energy. Here we assess each scheme's (explicit or implicit) subgrid model in terms of its spectral energy and enstrophy transfers. We evaluate the effects of different backscatter models/energy fixers on these transfers, on the accuracy of the vorticity field and on the long-term energy and enstrophy behaviour.

3. Spectral energy and enstrophy transfers

We use a high-resolution numerical solution of the barotropic vorticity equation to diagnose the effects on the energy and enstrophy tendency, as a function of wave number, of scales smaller than some specified truncation scale. These results provide reference values determining the ideal effects of the subgrid model (whether it be explicit or implicit) for a numerical model whose resolution is that truncation scale. We also diagnose the actual effects of the explicit or implicit subgrid models for the numerical schemes discussed in section 2 and compare these with the reference values.

3.1. Spin-up

The case analysed here is one of fully developed forced, dissipative, two-dimensional turbulence. The governing vorticity equation becomes

$$\frac{\partial \zeta}{\partial t} + \frac{\partial u\zeta}{\partial x} + \frac{\partial v\zeta}{\partial y} = F - \frac{\zeta}{\tau}, \tag{14}$$

where F is a fixed forcing given by

$$F = 0.1\sin(32\pi x), \tag{15}$$

and $\tau = 100$ is a large-scale dissipation time-scale (roughly 100 eddy turnover times). The spin up integration, as well as the reference calculation described below, used a spectral transform method, with alias-free calculation of quadratic terms, to integrate the governing equations. A ∇^8 dissipation was applied to the vorticity field with a time scale of 1 at the shortest retained scales. To allow the turbulence to come close to a statistical equilibrium, the solution was initialized with the vorticity field

$$\begin{aligned}\zeta = {} & \sin(8\pi x)\sin(8\pi y) \\ & + 0.4\cos(6\pi x)\cos(6\pi y) \\ & + 0.3\cos(10\pi x)\cos(4\pi y) \\ & + 0.02\sin(2\pi y) + 0.02\sin(2\pi x)\end{aligned} \tag{16}$$

and integrated for 180 time units on a 512×512 grid (maximum retained wave number 170), followed by 20 time units on a 2048×2048 grid (maximum retained wave number 682). The resulting spun-up vorticity field is shown in Figure 1. The figure gives an impression of the typical scales of motion, as well as a qualitative picture of the turbulent dynamics, showing merger

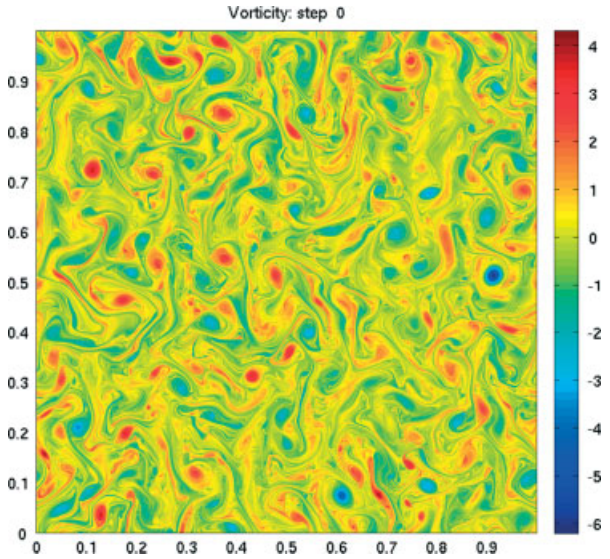

Figure 1. High-resolution vorticity field at the end of the spin-up integration. Red indicates positive vorticity; blue indicates negative vorticity.

of like-signed vortices, propagation of pairs of opposite-signed vortices, and stripping of vorticity filaments from vortices and their elongation and thinning in the turbulent strain field. The spun-up state was spectrally truncated to a range of different resolutions and used as the initial condition for the calculations described below.

3.2. *Reference calculation*

Retaining the forcing and dissipation terms in Eq. (14), the solution was integrated from the spun-up state for a further 10 time units at 2048×2048 resolution. For this reference integration, the spectral energy and enstrophy tendencies due to small scales are calculated as follows. At each time step we know the Fourier transforms of the vorticity $\hat{\zeta}(\mathbf{k})$ and the stream function $\hat{\psi}(\mathbf{k}) = -\hat{\zeta}(\mathbf{k})/|\mathbf{k}|^2$, where $\mathbf{k}$ is the wave number. First the energy and enstrophy tendency at every wave number are calculated for the full-resolution data. This is done by transforming ζ and ψ and their spatial derivatives to grid space, calculating the Jacobian

$$J(\mathbf{x}) = \nabla.(\mathbf{v}\zeta) = \frac{\partial\psi}{\partial x}\frac{\partial\zeta}{\partial y} - \frac{\partial\psi}{\partial y}\frac{\partial\zeta}{\partial x} \tag{17}$$

on the transform grid and transforming back to spectral space to obtain $\hat{J}(\mathbf{k})$, ($\hat{J}$ is truncated to the maximum retained wave number, 682×682 in our example, to avoid aliasing), then computing

$$\dot{E}(\mathbf{k}) = \mathrm{Re}\left\{\frac{\hat{\psi}^*(\mathbf{k})\hat{J}(\mathbf{k})}{\Delta k^2 N^4}\right\}, \tag{18}$$

$$\dot{Z}(\mathbf{k}) = -\mathrm{Re}\left\{\frac{\hat{\zeta}^*(\mathbf{k})\hat{J}(\mathbf{k})}{\Delta k^2 N^4}\right\}, \tag{19}$$

and finally integrating over angle in spectral space to obtain $\dot{E}(k)$ and $\dot{Z}(k)$. Here the superscript $*$ indicates a complex conjugate, $k = |\mathbf{k}|$, N is the grid resolution (2048 in our example), Δk is the wave number interval in spectral space, and the factor $\Delta k^2 N^4$ arises from the normalization of the Fourier transforms. The integral over angle in wave number space is carried out by dividing k-space into a number of bins of interval size Δk, assigning each discrete value of $\mathbf{k}$ to the appropriate k-bin and summing the values of $\dot{E}(\mathbf{k})$ and $\dot{Z}(\mathbf{k})$ in each bin, and multiplying the sum by Δk to obtain the correct normalization. Second, the $\hat{\zeta}$ and $\hat{\psi}$ data are truncated to retain only those spectral components with $k < k_T$ for some truncation wave number k_T, and the calculation of the spectral energy and enstrophy tendencies is repeated to give $\dot{E}_T(k)$ and $\dot{Z}_T(k)$. Finally, the contribution mediated by wave numbers greater than or equal to k_T is given by

$$\dot{E}_{\mathrm{SG}}(k) = \dot{E}(k) - \dot{E}_T(k), \tag{20}$$

$$\dot{Z}_{\mathrm{SG}}(k) = \dot{Z}(k) - \dot{Z}_T(k). \tag{21}$$

These contributions are averaged over the 10 time units of the reference integration.

Figure 2 shows the results of this calculation for three different truncation wave numbers: $k_T = 42,\ 85,\ 170$. The three $\dot{Z}_{\mathrm{SG}}$ plots show that the truncated scales remove enstrophy from wave numbers k smaller than but very close to k_T. The magnitude of the signal decreases as k_T increases, but the qualitative picture remains unchanged.

The three $\dot{E}_{\mathrm{SG}}$ plots show that the truncated scales also remove energy from wave numbers close to, but smaller than, k_T. However, they also transfer energy to large scales, to those wave numbers that are already most energetic. This is the signal of energy backscatter. Again, the magnitude of the signal decreases as k_T increases, but the qualitative picture remains unchanged. We have found this signal to be very robust. Repeating the calculation for a single time step produces very similar plots to those shown. A qualitatively similar picture is seen even for rather idealized flows that are far from fully developed turbulence, and for unforced freely decaying turbulent flow.

These results are consistent with, and can be understood in terms of, current understanding of the mechanisms for the downscale enstrophy transfer and upscale energy transfer in two-dimensional turbulence (e.g. Batchelor, 1969; Kraichnan, 1975, 1976; Rhines, 1979; Salmon, 1998; Chen *et al.*, 2003, 2006). Downscale enstrophy transfer across some wave number k_T is associated with straining and thinning of eddies with wave number $k \approx k_T$ (in this sense the transfer is local in wave number space) by the large-scale strain field, which is dominated by the largest flow scales, and occurs predominantly in the strain-dominated, rather than vorticity-dominated, regions of the flow. On the other hand, upscale energy transfer across wave number k_T is associated with thinning and tilting of eddies of smaller-scale, predominantly (but not exclusively) $4k_T$–$8k_T$ (in this sense the transfer is only weakly local in wave number space), by eddies of wave number comparable to k_T. This effect is stronger for smaller k_T simply because the larger scales are more energetic; hence the strongest energy input $\dot{E}_{\mathrm{SG}}$ in Figure 2 is to the largest, most energetic, scales.

The results in Figure 2 provide a reference solution against which to compare explicit or implicit subgrid models. Ideally, the subgrid model for a numerical solution with maximum resolved wave number k_T should be able to reproduce $\dot{E}_{\mathrm{SG}}$ and $\dot{Z}_{\mathrm{SG}}$ for the same k_T.

3.3. *Subgrid models*

In this section we compare several of the explicit and implicit subgrid models outlined in section 2 against the reference solution found above in terms of their spectral energy and enstrophy transfers. The final state of the spin-up integration is spectrally truncated to wave number k_T before integrating for a further 10 time units with the chosen scheme on a corresponding $N \times N$ coarse grid, where $N = 3k_T + 1$ or $3k_T + 2$. As for the reference integration, the forcing and dissipation terms in Eq. (14) are included. We present results for $k_T = 85$; other values of k_T (not shown) lead to the same conclusions.

The spectral energy and enstrophy tendencies due to the explicit or implicit subgrid model of the chosen scheme are diagnosed as follows. At each time step, the vorticity tendency $\dot{\zeta}(\mathbf{x})$ is computed using the chosen scheme including any explicit subgrid model. The vorticity tendency is also calculated using a spectral method (with no explicit dissipation term) at the same resolution: $\dot{\zeta}_{\mathrm{sp}}(\mathbf{x})$. Since the spectral method is an exact spatial discretization on

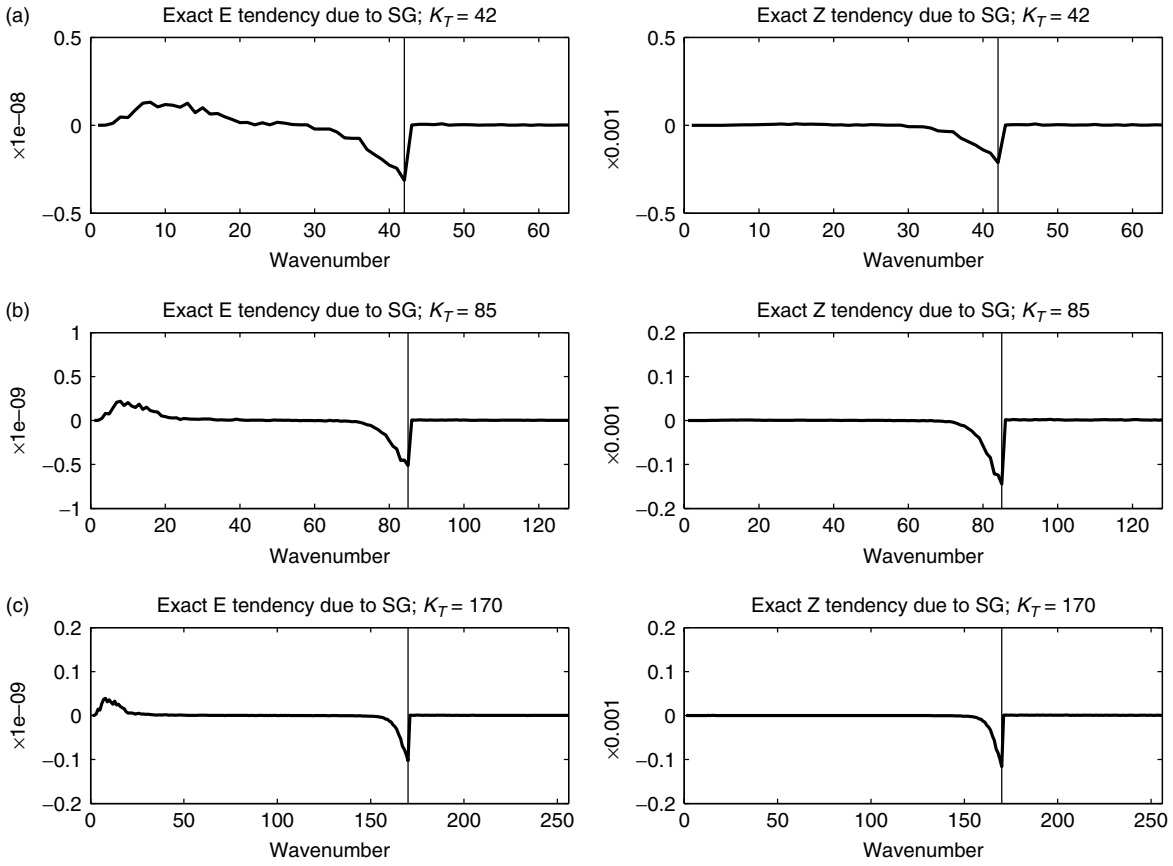

Figure 2. Spectral tendencies of energy $\dot{E}_{\mathrm{SG}}(k)$ (left) and enstrophy $\dot{Z}_{\mathrm{SG}}(k)$ (right) mediated by wave numbers greater than or equal to k_T. Top: $k_T = 42$; middle $k_T = 85$; bottom: $k_T = 170$. Note the different axis scales for the different values of k_T.

the retained scales, the difference $\dot{\zeta}_{\mathrm{SG}}(\mathbf{x}) = \dot{\zeta}(\mathbf{x}) - \dot{\zeta}_{\mathrm{sp}}(\mathbf{x})$ gives the vorticity tendency associated with the spatial truncation errors of the scheme plus any explicit subgrid model. Then $J_{\mathrm{SG}}(\mathbf{x}) = -\dot{\zeta}_{\mathrm{SG}}(\mathbf{x})$ is the contribution to the Jacobian from the effective subgrid model. $J_{\mathrm{SG}}(\mathbf{x})$ is transformed to spectral space to give $\hat{J}_{\mathrm{SG}}(\mathbf{k})$, and $\hat{J}(\mathbf{k})$ is replaced by $\hat{J}_{\mathrm{SG}}(\mathbf{k})$ in Eqs (18) and (19) to give spectral energy and enstrophy tendencies due to the effective subgrid model. Finally, these tendencies are integrated over angle in wave number space to obtain $\dot{E}_{\mathrm{SG}}(k)$ and $\dot{Z}_{\mathrm{SG}}(k)$. These diagnostics are averaged over the 10 time units of the integration.

Figure 3 shows the spectral energy and enstrophy tendencies due to the simple, explicit ∇^4 and ∇^8 hyperdiffusion subgrid models in the spectral method. A ∇^4 subgrid model removes enstrophy predominantly from large wave numbers, but is much less scale-selective than the reference solution. The magnitude of the spectral energy tendency actually increases towards smaller wave numbers until the forcing scale ($k = 16$) is reached. Importantly, energy is removed at all wave numbers; there is no representation of the backscatter. A ∇^8 subgrid model is more scale-selective, but still significantly less so than the reference solution. Again, there is no representation of backscatter.

The above results suggest that an even more scale-selective hyperdiffusion (∇^{2n} with $n > 4$) might give spectral energy and enstrophy sink profiles even closer to the reference values. However, if we retain a dissipation time-scale of one time unit at the shortest resolved scale then the shortest scales are so strongly damped that further enstrophy transfer to those scales is inhibited, with the result that enstrophy builds up at slightly larger scales and the dissipation moves to those larger scales. If, on the other hand, we increase the dissipation time-scale significantly (say by a factor 10), then we do indeed see dissipation concentrated at a much sharper range of wave numbers, more like the reference results; however, the enstrophy dissipation is then insufficient and the vorticity field becomes noisy. Careful tuning is needed to find the optimal compromise between these cases. The fact that the optimal tuning will be flow dependent is a well-known limitation of tunable dissipation schemes.

Figure 4 shows the spectral energy and enstrophy tendencies for the effective subgrid model of the Arakawa Jacobian combined with an explicit ∇^4 or ∇^8 hyperdiffusion term. The most striking feature is an energy and enstrophy source at the forcing wave number. (A similar feature is found for other centred second order schemes, such as the individual Jacobians from which the Arakawa Jacobian is built – not shown). Examination of $\dot{E}(k)$ and $\dot{E}_{\mathrm{sp}}(k)$ shows that both have a sink of around 0.15×10^{-6} at the forcing wave number, needed to balance the energy input by the forcing. The spike seen in Figure 4 shows that the Arakawa Jacobian underestimates this sink by about 3%. The figure also shows that the Arakawa Jacobian's effective subgrid model removes energy from scales larger than the forcing scale. Again, examination of $\dot{E}(k)$ and $\dot{E}_{\mathrm{sp}}(k)$ shows that this really indicates a slight underestimation of the upscale energy transfer by the Arakawa Jacobian compared with the reference spectral method. Both of these features become much smaller at higher resolution (by roughly a factor 1/4 when the spatial resolution is doubled), confirming that they are associated with the truncation errors of the Arakawa Jacobian. The effect of the ∇^4 and ∇^8 hyperdiffusion terms on the medium and small scales are similar to the spectral case shown in Figure 3.

Figure 5 shows the effect of truncation errors on the spectral energy and enstrophy tendencies when UTOPIA is used for advection of vorticity. For a constant advecting velocity, UTOPIA is third-order accurate (Leonard *et al.*, 1993), so its truncation errors involve fourth spatial derivatives. Therefore, its implicit subgrid model is expected to behave in a qualitatively similar way to an explicit ∇^4 hyperdiffusion. The results show that UTOPIA's truncation errors remove enstrophy at a similar rate across a broad range of scales. Its implied subgrid model appears to be even less selective of small scales than an explicit ∇^4 hyperdiffusion. UTOPIA's truncation errors lead to an upscale energy transfer from around the forcing scale ($k \approx 16$) to larger

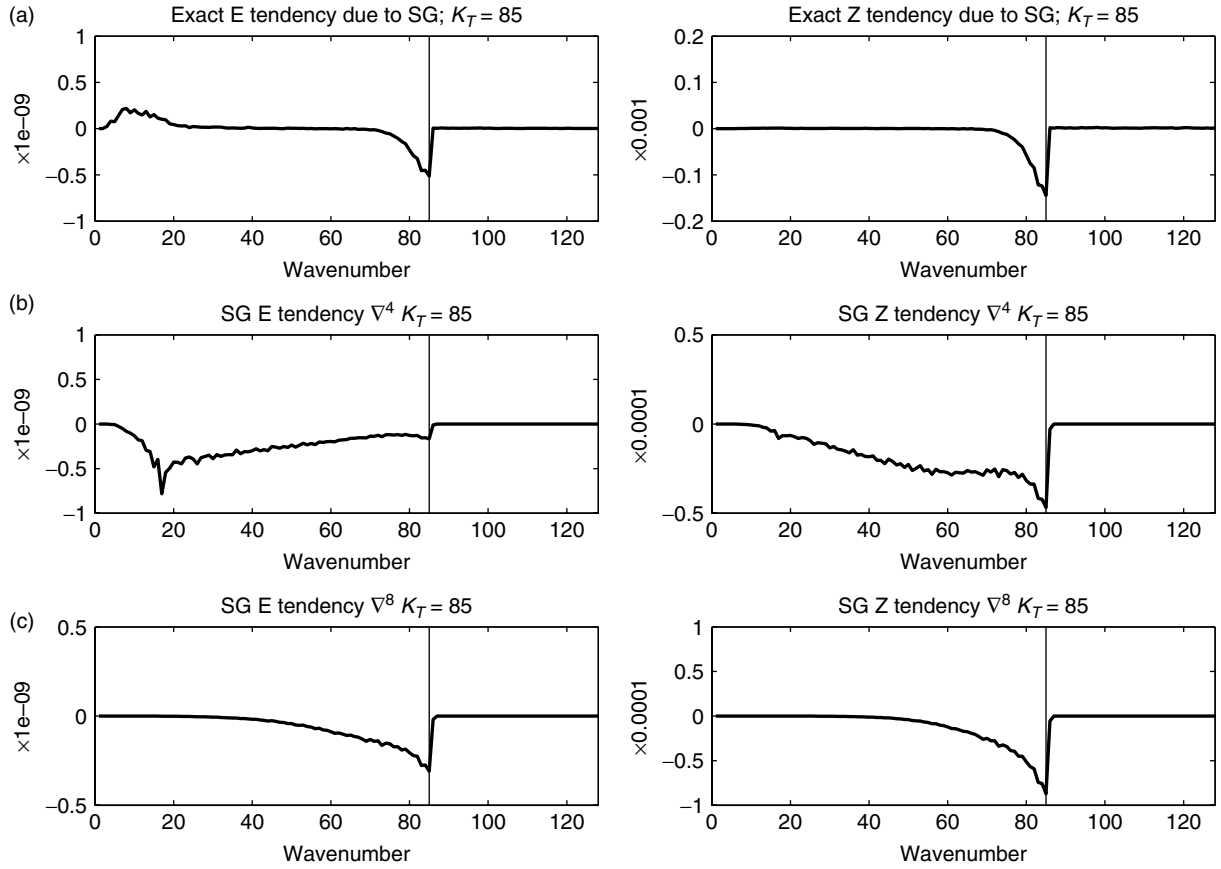

Figure 3. Top: $\dot{E}_{SG}(k)$ and $\dot{Z}_{SG}(k)$ for $k_T = 85$ (same as the middle row of Figure 2). Middle: $\dot{E}_{SG}(k)$ and $\dot{Z}_{SG}(k)$ for a ∇^4 subgrid model. Bottom: $\dot{E}_{SG}(k)$ and $\dot{Z}_{SG}(k)$ for a ∇^8 subgrid model.

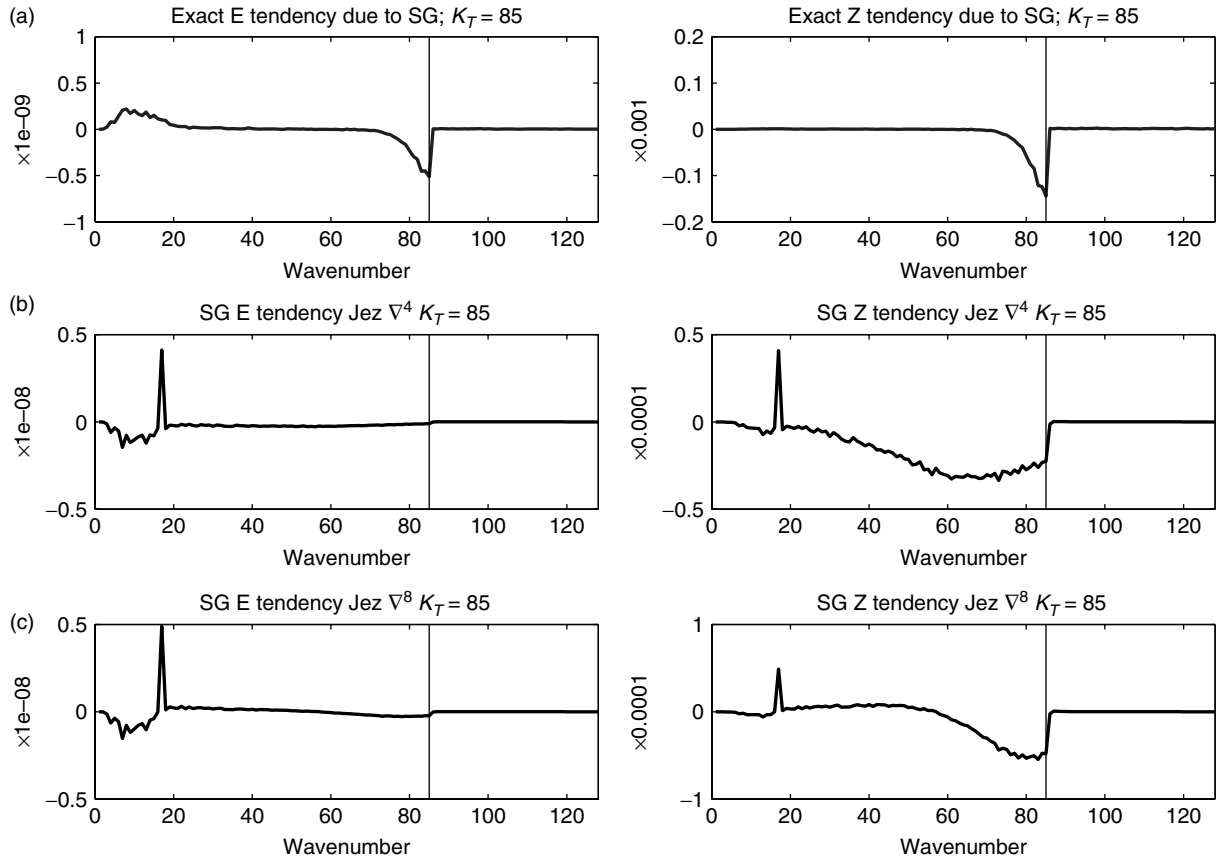

Figure 4. Top: $\dot{E}_{SG}(k)$ and $\dot{Z}_{SG}(k)$ for $k_T = 85$ (same as the middle row of Figure 2). Middle: $\dot{E}_{SG}(k)$ and $\dot{Z}_{SG}(k)$ for the Arakawa Jacobian with a ∇^4 hyperdiffusion. Bottom: $\dot{E}_{SG}(k)$ and $\dot{Z}_{SG}(k)$ for the Arakawa Jacobian with a ∇^8 hyperdiffusion.

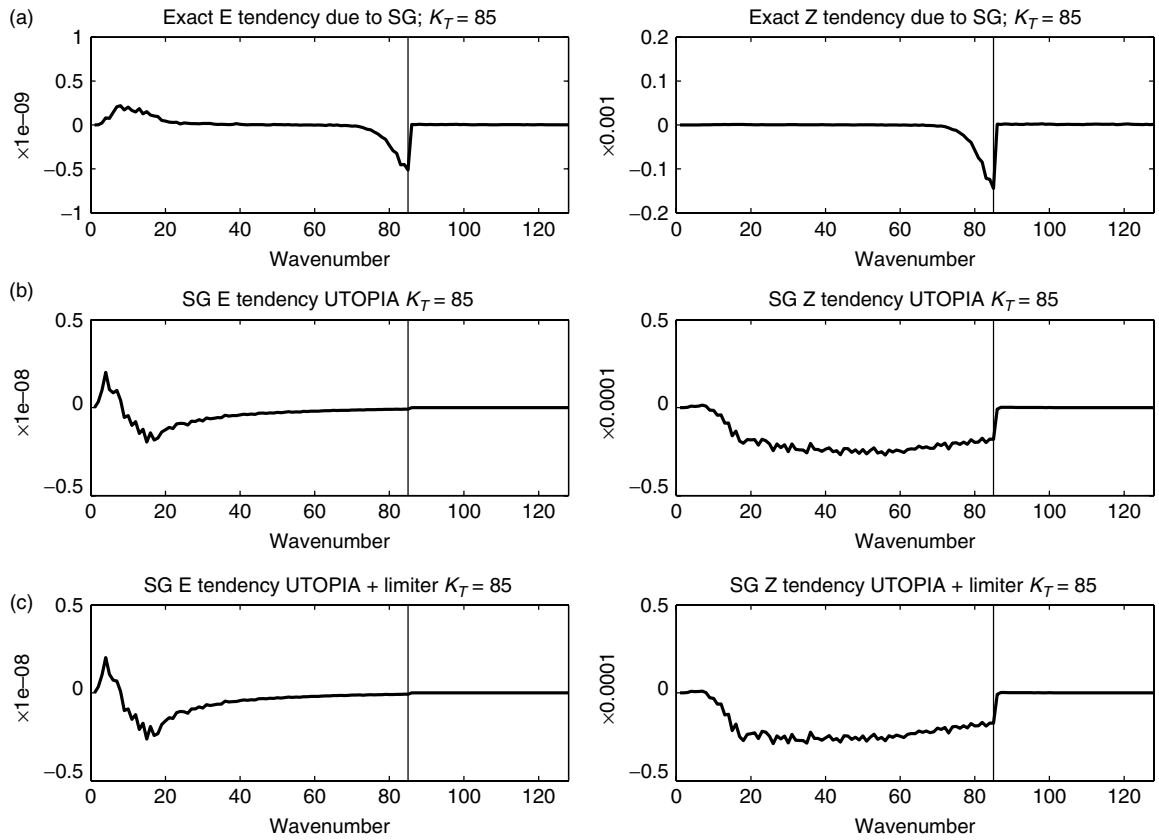

Figure 5. Top: $\dot{E}_{\mathrm{SG}}(k)$ and $\dot{Z}_{\mathrm{SG}}(k)$ for $k_T = 85$ (same as the middle row of Figure 2). Middle: $\dot{E}_{\mathrm{SG}}(k)$ and $\dot{Z}_{\mathrm{SG}}(k)$ for the truncation errors of the UTOPIA scheme. Bottom: $\dot{E}_{\mathrm{SG}}(k)$ and $\dot{Z}_{\mathrm{SG}}(k)$ for the truncation errors of the flux-limited UTOPIA scheme.

scales ($k \approx 5$). These spectral energy sources and sinks are an order of magnitude larger than the reference solution backscatter signal. The inclusion of a flux limiter makes a negligible difference to the results.

Figure 6 shows the spectral energy and enstrophy tendencies due to the two versions of the APVM subgrid model. For the D_2 version of the scheme, there is indeed a net removal of enstrophy while the total energy is conserved. Consistent with this, there is a net upscale transfer of energy; however, this transfer is fairly local in wave number space, in contrast to the reference solution, in which the energy transfer is very nonlocal. Although there is some preference for enstrophy removal to occur at the smallest scales, it is significant across most of the spectrum. Moreover, when the coefficient θ is tuned so that the peak energy source is comparable to the reference solution (as here), the enstrophy removal is an order of magnitude smaller than for the reference solution. As a result, vorticity maps show the emergence of grid-scale noise.

The patterns of spectral energy and enstrophy transfers for the D_2 version of APVM show a striking resemblance to those for UTOPIA. A possible explanation for this is that the D_2 version of APVM can be interpreted in terms of an upwind scheme for the advection of vorticity. Further investigation of this similarity might provide valuable insight.

The D_4 version of the scheme gives a more scale-selective enstrophy sink, though still not as scale-selective as the reference solution, while conserving energy. The energy transfers are more non-local than for the D_2 version and more similar to the reference values. However, the size of the enstrophy sink remains an order of magnitude too small.

The diagnostics presented above were also calculated for a single time step. The single-step diagnostics typically showed more dissipation at small scales than the time-averaged diagnostics. Kent *et al.* (2012) showed that when a coarse-resolution model is restarted from coarse-grained higher-resolution data, as here, there is a short adjustment period of a few eddy turnover times during which enstrophy is rapidly removed and the energy spectrum adjusts to the new scheme and/or resolution. Therefore, the time-averaged diagnostics presented above are expected to be more representative of the long-term behaviour of the chosen schemes.

4. Energy conservation and backscatter

Figures 3–6 show two features of the spectral energy budget of typical schemes and their subgrid models that could be improved. One is the failure to represent correctly the true energy backscatter to large scales; the other is excessive energy and enstrophy dissipation over the middle range of the spectrum. Here we propose a simple and computationally cheap scheme that can potentially address both of these issues, based on amplifying chosen scales in the existing vorticity field. We show below that the proposed scheme gives energy conservation without adversely affecting enstrophy dissipation, and in some cases leads to a small improvement in the accuracy of the vorticity field. Any more elaborate scheme would need to be justified by a firm theoretical basis or by a demonstration that it is more accurate in practice.

4.1. *Backscatter/energy fixer scheme*

The backscatter/energy fixer scheme works as follows. At each time step a preliminary solution is calculated using the chosen numerical method and its subgrid model (but without the inclusion of any large-scale forcing or dissipation), which should be enstrophy-dissipating. The preliminary solution will then almost certainly have less energy than the solution at the previous time step. The lost energy is restored by adding a suitable vorticity perturbation to the preliminary vorticity field.

We choose a vorticity pattern that is based on a filtered form of the predicted vorticity field, which we justify as follows. To a first approximation, the true backscatter tends to amplify the existing large-scale vorticity pattern, consistent with the diagnostics presented in section 3.3 and the current understanding of two-dimensional turbulence discussed at the end of section

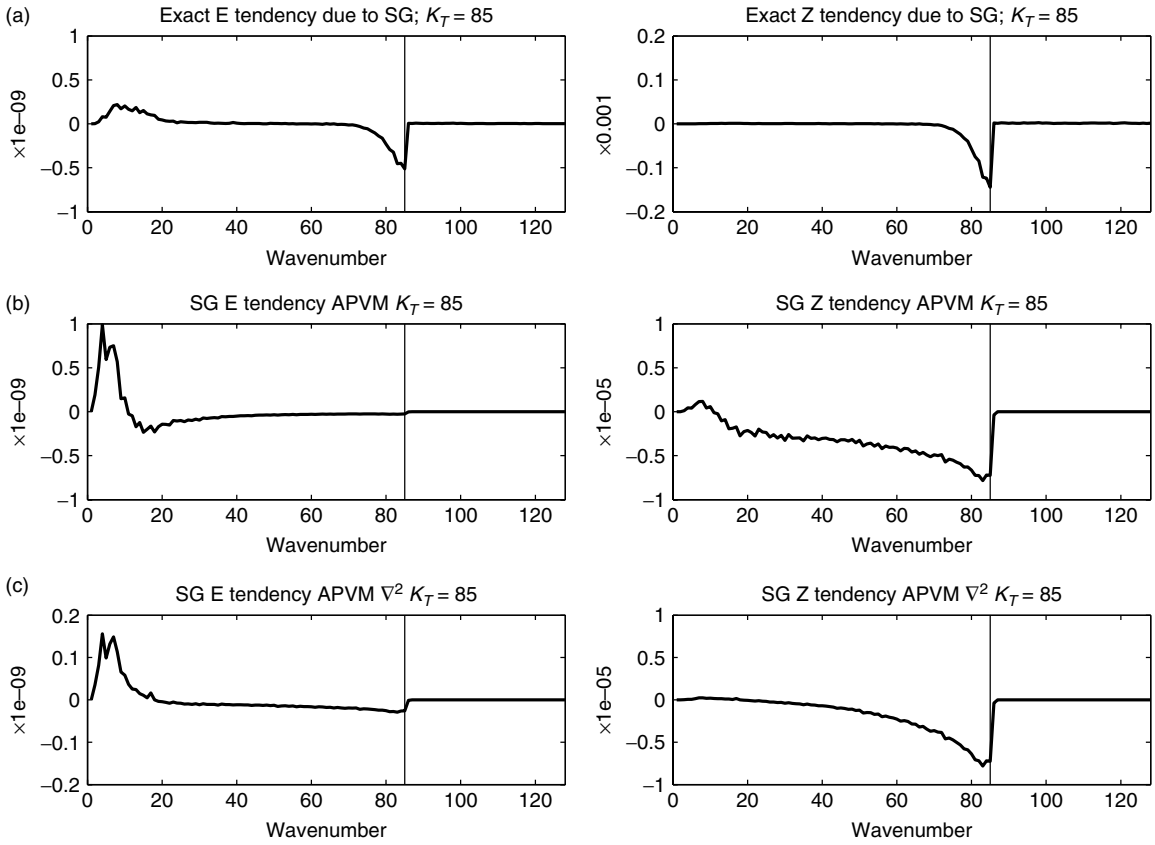

Figure 6. Top: $\dot{E}_{SG}(k)$ and $\dot{Z}_{SG}(k)$ for $k_T = 85$ (same as the middle row of Figure 2). Middle: $\dot{E}_{SG}(k)$ and $\dot{Z}_{SG}(k)$ for the D_2 APVM. Bottom: $\dot{E}_{SG}(k)$ and $\dot{Z}_{SG}(k)$ for the D_4 APVM.

3.2. At the same time, imperfect subgrid models, such as low-order hyperdiffusion, tend to damp excessively the small and intermediate scales of the existing vorticity pattern. Finally, advection schemes considered suitable for ILES are those whose dominant truncation errors are associated with damping of the advected field on small and intermediate scales (rather than dispersion errors). In all cases the argument implies that it should be possible to improve the solution by amplifying a suitable range of scales in the vorticity spectrum. It is notable that the proposed scheme is completely deterministic.

The general form of the backscatter/energy fixer scheme is

$$\zeta^{n+1} = \zeta^P + \alpha\,\delta\zeta, \tag{22}$$

where ζ^P is the preliminary solution for step $n+1$, $\delta\zeta$ is the vorticity pattern to be added and α is the amplitude of the vorticity pattern to be added.

Although the true backscatter need not exactly conserve the energy on scales $k < k_T$ (e.g. see Figure 9), it very nearly does so. For simplicity, and to avoid the potential for instability if we allow the resolved energy to grow, the proposed scheme is designed to conserve energy almost exactly as a first approximation to the true behaviour. To ensure energy conservation, α must be chosen such that the energy at the new time step equals the energy at the current time step (denoted E_0). Equating the desired energy to the energy associated with the modified vorticity gives

$$E_0 = -\frac{1}{2}\int (\zeta^P + \alpha\delta\zeta)(\psi^P + \alpha\delta\psi)\,\mathrm{d}A \tag{23}$$

Integrating by parts twice and assuming that α is small gives

$$E_0 = -\frac{1}{2}\int \zeta^P\psi^P + 2\alpha\delta\zeta\,\psi^P\,\mathrm{d}A. \tag{24}$$

The energy calculated from the preliminary solution is

$$E_P = -\frac{1}{2}\int \zeta^P\psi^P\,\mathrm{d}A, \tag{25}$$

and therefore Eq. (24) can be rearranged to give

$$\alpha = \frac{E_P - E_0}{\int \delta\zeta\,\psi^P\,\mathrm{d}A}. \tag{26}$$

Therefore, for a given $\delta\zeta$ we can calculate the value of α needed to give energy conservation. (Because $\delta\zeta$ is derived from a filtered form of the preliminary ζ field, there is no danger that the denominator in Eq. (26) will vanish.) It should be noted that the proposed scheme will have no effect on the APVM (or any other energy conserving method) because Eq. (26) will imply $\alpha = 0$.

The choice of $\delta\zeta$ determines the pattern of vorticity that will be added to the solution. It is important in ensuring that energy is added to an appropriate place in physical space, and an appropriate wave number in spectral space. The optimal choice of vorticity pattern will depend on the preliminary scheme used. We have not rigorously optimized $\delta\zeta$ (which would involve a complicated optimization problem), but we have experimented with several vorticity patterns of the form

$$\delta\zeta = \nabla^{2n}\zeta, \tag{27}$$

with $n = -1, 0, 1, 2$ and of the form

$$\delta\zeta = \overline{\zeta}^L \tag{28}$$

and

$$\delta\zeta = \zeta - \overline{\zeta}^L, \tag{29}$$

where an overline indicates a two-dimensional uniform spatial average over an $L \times L$ region with $L = 2\Delta x$ or $4\Delta x$. The proposed scheme was originally conceived as a representation of the missing energy backscatter to large scales, for which a large scale $\delta\zeta$ pattern would be appropriate, given by Eq. (28) or by Eq. (27) with $n = -1$ or $n = 0$. However, for many schemes, energy errors in the mid to high wave number range are more significant than the missing backscatter, and fixing these requires a smaller-scale $\delta\zeta$ pattern given by Eq. (29) or by Eq. (27) with $n = 1$ or $n = 2$.

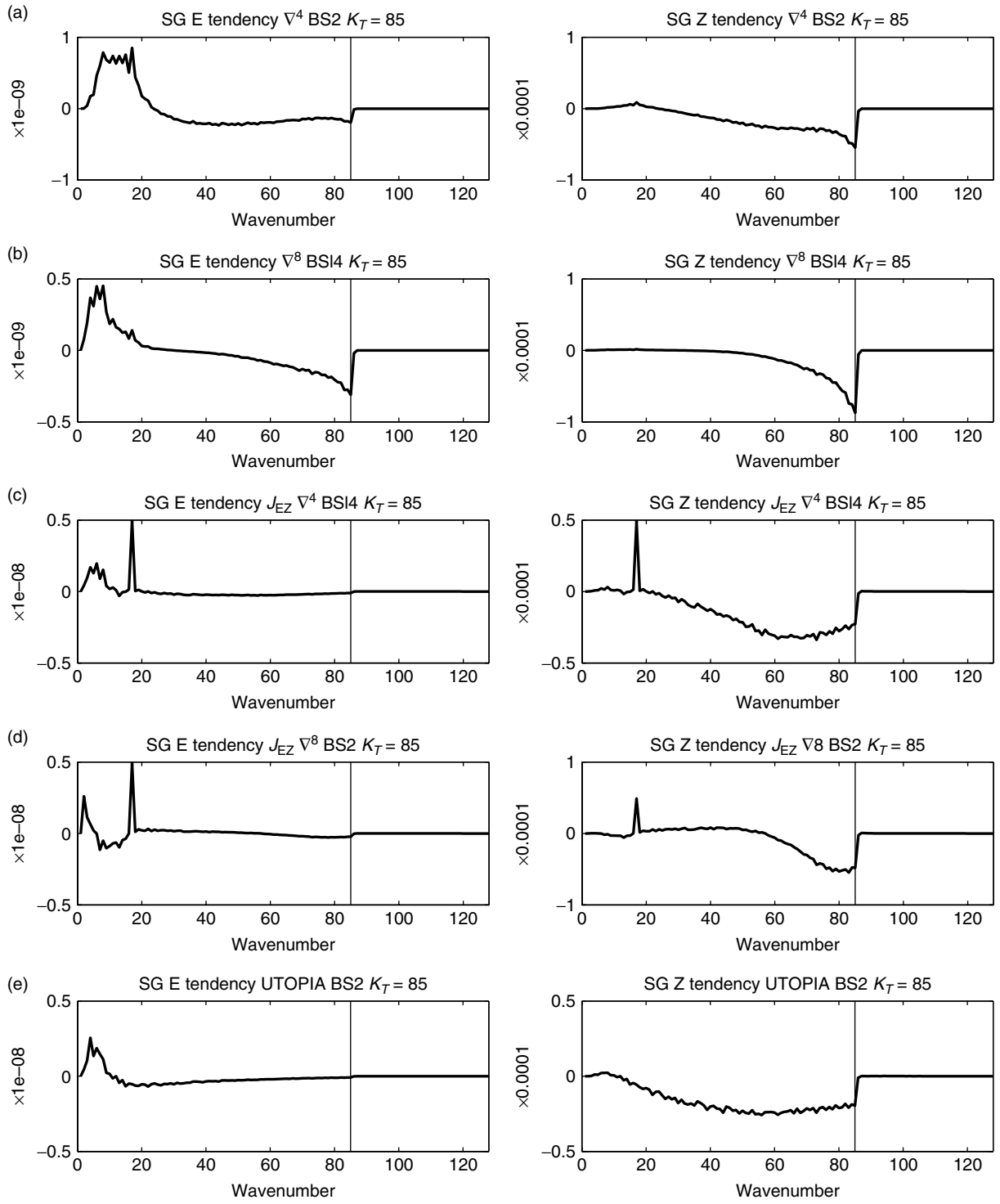

Figure 7. Spectral energy transfers $\dot{E}_{\mathrm{SG}}(k)$ (left) and enstrophy transfers $\dot{Z}_{\mathrm{SG}}(k)$ (right) for the effective subgrid models of several schemes with example backscatter/energy fixer models for $k_T = 85$. Row 1: spectral method with ∇^4 hyperdiffusion and $\delta\zeta = \nabla^2\zeta$. Row 2: spectral method with ∇^8 hyperdiffusion and $\delta\zeta = \overline{\zeta}^{4\Delta x}$. Row 3: Arakawa Jacobian with ∇^4 hyperdiffusion and $\delta\zeta = \overline{\zeta}^{4\Delta x}$. Row 4: Arakawa Jacobian with ∇^8 hyperdiffusion and $\delta\zeta = \nabla^{-2}\zeta$; Row 5: UTOPIA with $\delta\zeta = \nabla^2\zeta$.

5. Numerical results

In this section the effects of the proposed backscatter model/energy fixer are investigated using a variety of numerical experiments and diagnostics.

5.1. Spectral energy and enstrophy transfers

For each preliminary scheme and choice of $\delta\zeta$, the spectral energy and enstrophy transfers associated with the effective subgrid model were computed, as in section 3.3. Figure 7 shows results for a selection of schemes. For each preliminary scheme, results are shown for the choice of $\delta\zeta$ that gave the smallest l_2 vorticity error for the test described in section 5.2. These results should be compared with those in the absence of a backscatter model/energy fixer, and the reference solutions, shown in section 3.3.

5.2. Vorticity errors

By improving the representation of spectral energy and enstrophy transfers we might hope to improve the accuracy of the solution for vorticity itself, or at least not make it less accurate. The effect on accuracy was assessed by solving a freely decaying turbulence initial value problem. The initial condition was the same as that used for the reference integration in section 3.2 and the experiments described in sections 3.3 and 5.1. However,

Table 1. l_2 vorticity errors for the freely decaying turbulence test at time 10. J_{EZ} indicates the Arakawa energy and enstrophy-conserving Jacobian; the other notation is defined in the main text.

Preliminary scheme	None	$\delta\zeta = \nabla^{-2}\zeta$	$\delta\zeta = \zeta$	$\delta\zeta = \nabla^2\zeta$	$\delta\zeta = \nabla^4\zeta$
Spectral ∇^4	0.2634	0.2815	0.2636	**0.2532**	0.4593*
Spectral ∇^8	**0.2398**	0.2416	**0.2403**	0.2429	0.2717
Spectral ∇^{12}	**0.2337**	0.2351	**0.2341**	0.2361	0.2506
$J_{EZ} + \nabla^4$	0.3885	0.3854	**0.3832**	0.3960	3.5687**
$J_{EZ} + \nabla^8$	0.4339	**0.4315**	0.4327	0.4412	0.4702
UTOPIA	0.2788	0.2940	0.2785	**0.2678**	0.4148**
UTOPIA+limiter	0.2855	0.3173	0.2846	**0.2685**	0.6071**
APVM D_2	0.3571				
APVM D_4	0.3285				

Table 2. l_2 vorticity errors for the freely decaying turbulence test at time 10. J_{EZ} indicates the Arakawa energy and enstrophy-conserving Jacobian; the other notation is defined in the main text.

Preliminary scheme	$\delta\zeta = \overline{\zeta}^{2\Delta x}$	$\delta\zeta = \overline{\zeta}^{4\Delta x}$	$\delta\zeta = \zeta - \overline{\zeta}^{2\Delta x}$	$\delta\zeta = \zeta - \overline{\zeta}^{4\Delta x}$
Spectral ∇^4	0.2638	0.2641	0.2541	0.2557
Spectral ∇^8	0.2403	**0.2402**	0.2425	0.2420
Spectral ∇^{12}	0.2341	**0.2340**	0.2359	0.2356
$J_{EZ} + \nabla^4$	0.3830	**0.3828**	0.3951	0.3936
$J_{EZ} + \nabla^8$	0.4326	0.4324	0.4404	0.4392
UTOPIA	0.2787	0.2790	0.2686	0.2699
UTOPIA+limiter	0.2848	0.2853	0.2693	0.2713

the subsequent evolution was computed with the forcing and large-scale dissipation terms switched off by setting $F = 0$ and $1/\tau = 0$. (This makes it easier to investigate the behaviour of the maximum vorticity, section 5.3, and to check conservation of energy.) A high-resolution spectral solution (2048 × 2048) with ∇^8 hyperdiffusion was used to compute a reference solution at time $t = 10$, which was then spectrally truncated to 256 × 256 resolution. The initial data were then truncated to 256 × 256 resolution and integrated to $t = 10$ using a variety of preliminary schemes and $\delta\zeta$ patterns. The l_2 (root mean square) vorticity errors were calculated relative to the truncated reference solution. (Visual comparison of the vorticity solutions from all of the integrations confirmed that the solution is predictable, rather than chaotic, out to at least $t = 10$, and therefore the l_2 vorticity errors are meaningful.) The results are shown in Tables 1 and 2. For each preliminary scheme, the $\delta\zeta$ pattern (or patterns) giving the smallest error are indicated in bold. For comparison, the l_2 errors for the two versions of the APVM are also included; for these tests the coefficient θ was 10 times the value used in section 3.3 to provide better control of small-scale noise.

Before considering the effects of the backscatter model/energy fixer, the following point is noteworthy. For the spectral method, a ∇^8 hyperdiffusion is more accurate than a ∇^4 hyperdiffusion (and a ∇^{12} hyperdiffusion is more accurate again). This is consistent with the fact that the spectral method is very accurate for the resolved scales (spatial derivatives are calculated exactly), while the more scale-selective hyperdiffusion better mimics the true effects of subgrid scales (Figure 3). On the other hand, for the Arakawa Jacobian, a ∇^4 hyperdiffusion is more accurate than a ∇^8 hyperdiffusion. A plausible explanation is the following. The Arakawa Jabobian's truncation errors are second order, so that, when weighting by the shape of the spectrum is taken into account, they can be significant even at large and intermediate scales. Moreover, the errors are dispersive, and it is generally better to damp a feature than to represent it with the wrong phase. The less scale-selective ∇^4 hyperdiffusion is better able to control the intermediate scale dispersion errors than the ∇^8 hyperdiffusion.

We now turn our attention to the effects of the backscatter model/energy fixer. The most noticeable result is that the accuracy of the vorticity is dominated by the choice of preliminary scheme; in most cases the inclusion of a backscatter model/energy fixer has a relatively minor impact on the errors. Nevertheless, some clear signals emerge, and in most cases the inclusion of an appropriate backscatter model/energy fixer is able to reduce the errors.

For a preliminary scheme that is relatively accurate but lacking a representation of backscatter, such as the spectral method with ∇^8 or higher-order hyperdiffusion (see Figure 3), the most accurate results are obtained by using a large-scale $\delta\zeta$ pattern. The effect of the proposed scheme is to inject energy at scales similar to those at which the true backscatter injects energy (Figure 7, row 2). In this case it is legitimate to consider the proposed scheme to be a parametrization of backscatter. The l_2 errors are, however, marginally worse than the case without backscatter.

For the Arakawa Jacobian, with either ∇^4 or ∇^8 hyperdiffusion, again the best results are obtained with a large-scale $\delta\zeta$ pattern. However, in this case the proposed scheme is fixing errors in the energy spectrum at large scales associated with the truncation errors of the Arakawa Jacobian (compare Figure 7, rows 3 and 4 with Figure 4), rather than parametrizing the true backscatter.

For the spectral method with a ∇^4 hyperdiffusion, the excessive dissipation at intermediate scales (Figure 3) is a bigger source of error than the lack of a representation of backscatter. Hence the biggest gains in accuracy come from the choice of a pattern such as $\delta\zeta = \nabla^2\zeta$ that projects strongly onto intermediate scales (Figure 7 row 1).

The UTOPIA scheme (with or without a flux limiter) has significant spectral energy errors at both large and intermediate scales, with a spurious energy source at wave numbers smaller than about 10 and excessive dissipation at larger scales (Figure 5). The use of an energy fixer with an intermediate scale pattern such as $\delta\zeta = \nabla^2\zeta$ is able to compensate much of the excessive dissipation, and thereby significantly reduce vorticity errors, though a net upscale energy transfer, much larger than the true backscatter signal, remains (Figure 7).

Among all the schemes tested, the biggest reductions in l_2 vorticity error obtained through the energy fixer come from using a $\delta\zeta = \nabla^2\zeta$ pattern with the spectral plus ∇^4 scheme and with the UTOPIA schemes. Even in these cases the reduction in error is only in the region of 5%. Two factors help explain why the reduction in error is not larger. First, the errors are dominated by the marginally resolved scales, which are retained at full amplitude in the spectrally truncated reference solution, but are necessarily somewhat damped in all of the 256 × 256 resolution integrations. It appears unlikely that anything can be done to reduce this contribution to the error. Second, both

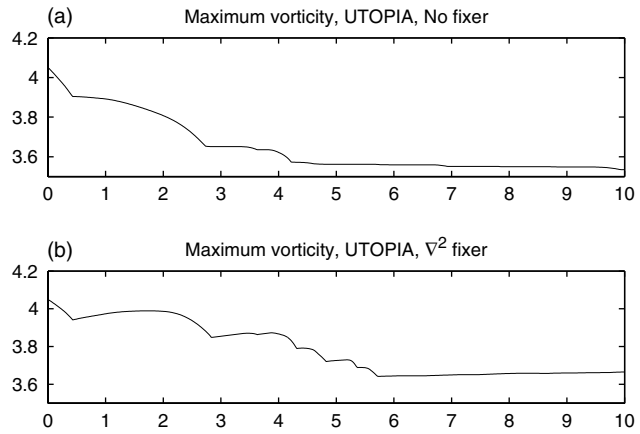

Figure 8. Time series of maximum vorticity for the experiments of section 5.2. Top: UTOPIA with flux limiter. Bottom: UTOPIA with flux limiter plus backscatter/fixer scheme with $\delta\zeta = \nabla^2\zeta$.

amplitude errors and position or dispersion errors contribute to the overall error. The proposed scheme can only be expected to reduce some of the amplitude errors.

Finally, note that it is important not to attempt to feed energy into scales smaller than or comparable to those at which it is removed by the preliminary scheme by choosing a $\delta\zeta$ that is too small scale. When using $\delta\zeta = \nabla^4\zeta$, the cases marked with '$*$' in Table 1 were somewhat noisy at small scales, while those marked with '$**$' acquired unphysical large-amplitude grid scale features. For the other cases in the tables, the backscatter/fixer scheme feeds energy into scales larger than those at which it is removed by the preliminary scheme; for these cases we have checked that the backscatter/fixer scheme does not introduce any unphysical flattening or upturn in the high wave number tail of the energy or enstrophy spectrum.

5.3. *Boundedness errors*

In the absence of forcing, local extrema in the vorticity field should not grow with time. A discrete analogue of this property is that the ζ value at any grid point should be bounded by the ζ values in some neighbourhood at the previous time step. However, the proposed backscatter/fixer scheme is not guaranteed to respect this boundedness property. It is therefore important to assess the size of any boundedness violations.

Of the preliminary schemes tested, only the UTOPIA scheme with limiter has this boundedness property. Figure 8 shows time series of the maximum vorticity in the domain for two of the experiments described in section 5.2: UTOPIA with limiter, and UTOPIA with limiter plus the $\delta\zeta = \nabla^2\zeta$ fixer. Without the fixer, the maximum vorticity decreases monotonically with time, as it should. The decrease is somewhat episodic. The effect of the fixer is to superpose a small, fairly steady, increasing trend on this episodic decrease. The net effect remains an overall decrease, and the boundedness violations are rather small. Whether these are important enough to invalidate the use of the proposed scheme will depend on the intended application.

The other preliminary schemes tested do not guarantee boundedness. (Indeed, hyperviscosity itself can create overshoots.) For these preliminary schemes, the effect of the backscatter/fixer scheme on the maximum vorticity was found to be small compared to the boundedness violations introduced by the preliminary scheme itself (not shown).

5.4. *Long-term energy and enstrophy conservation*

The effect of the proposed backscatter/fixer scheme on the long-term energy and enstrophy behaviour was examined using a freely decaying turbulence test case. The initial condition was the same as that used for the previous tests. As in section 5.2, we set $F = 0$ and $1/\tau = 0$. Time series of total energy and total enstrophy were computed up to $t = 100$ for a number of schemes at 256×256 resolution without the backscatter/fixer scheme, and also with the backscatter/fixer scheme that gave the lowest l_2 vorticity errors in section 5.2. For comparison, a high-resolution 2048×2048 reference run was also carried out, again using a spectral method with ∇^8 hyperdiffusion, and the energy and enstrophy at wave numbers $k < k_T = 85$ diagnosed. The results are shown in Figure 9.

Although the total energy of the reference run decreases slightly over time (not shown), the top panel in Figure 9 shows that the energy at wave numbers $k < k_T = 85$ actually increases after an initial dip, though only by about 0.1%. This is a manifestation of the expected upscale energy transfer or backscatter.

The middle row of panels in Figure 9 show that, with both the spectral method and the Arakawa Jacobian, a ∇^4 hyperdiffusion leads to significantly more energy dissipation (about 7%) than a ∇^8 hyperdiffusion (about 2%). The UTOPIA scheme is intermediate, giving about 5% total energy loss, while the UTOPIA scheme with flux limiter is most dissipative (about 9% total energy loss). Interestingly, for the UTOPIA scheme the total energy increases slightly during the last third of the run. In all cases the inclusion of the backscatter/fixer scheme leads to exact conservation of total energy, as designed.

The bottom row of panels in Figure 9 shows that the enstrophy at wave numbers $k < k_T = 85$ in the reference run decreases throughout the run, consistent with the expected downscale cascade. For all of the coarse resolution runs there is a qualitatively similar but greater enstrophy decrease. Schemes that dissipate most energy also dissipate most enstrophy. The inclusion of the backscatter/fixer scheme partly offsets the dissipation of enstrophy, though the effect is barely noticeable for the spectral ∇^8 and Arakawa Jacobian ∇^8 schemes. Even with the inclusion of the backscatter/fixer scheme, all of the coarse-resolution runs dissipate more enstrophy than the reference solution.

6. Conclusions

We have used a high-resolution turbulent solution of the barotropic vorticity equation to investigate the spectral energy and enstrophy transfers mediated by wave numbers greater than some truncation wave number k_T. Enstrophy is removed from a narrow range of wave numbers close to but smaller than k_T. Energy is also removed from these wave numbers but is fed back in at the scales that are already most energetic (backscatter). This signal is very robust for different k_T, different flow regimes, and even for single-step diagnostics. These diagnostics define the spectral energy and enstrophy tendencies required of an ideal subgrid model for a numerical solution with maximum resolved wave number $k_{\max} = k_T$.

For a selection of typical numerical schemes, the spectral energy and enstrophy transfers due to their effective subgrid model (i.e. the combined effects of numerical truncation errors and any explicit subgrid model) were diagnosed and compared with the ideal. The typical schemes are able to remove enstrophy and energy at small scales, but tend to do so over too wide a range of scales, resulting in excessive energy dissipation. Numerical truncation errors can lead to significant energy transfer errors at large scales. None of the schemes realistically represents the backscatter.

We propose a backscatter/energy fixer scheme that adds a vorticity perturbation to the solution at each time step. The pattern of the vorticity perturbation is defined to be a filtered version of the actual vorticity pattern, and its amplitude is determined to ensure energy conservation. Among the perturbation patterns tested, the best choice is found to depend strongly on the numerical scheme used. For an accurate numerical scheme, such as the spectral method with high-order hyperdiffusion, a large-scale vorticity perturbation leads to a realistic parametrization of energy backscatter, though the

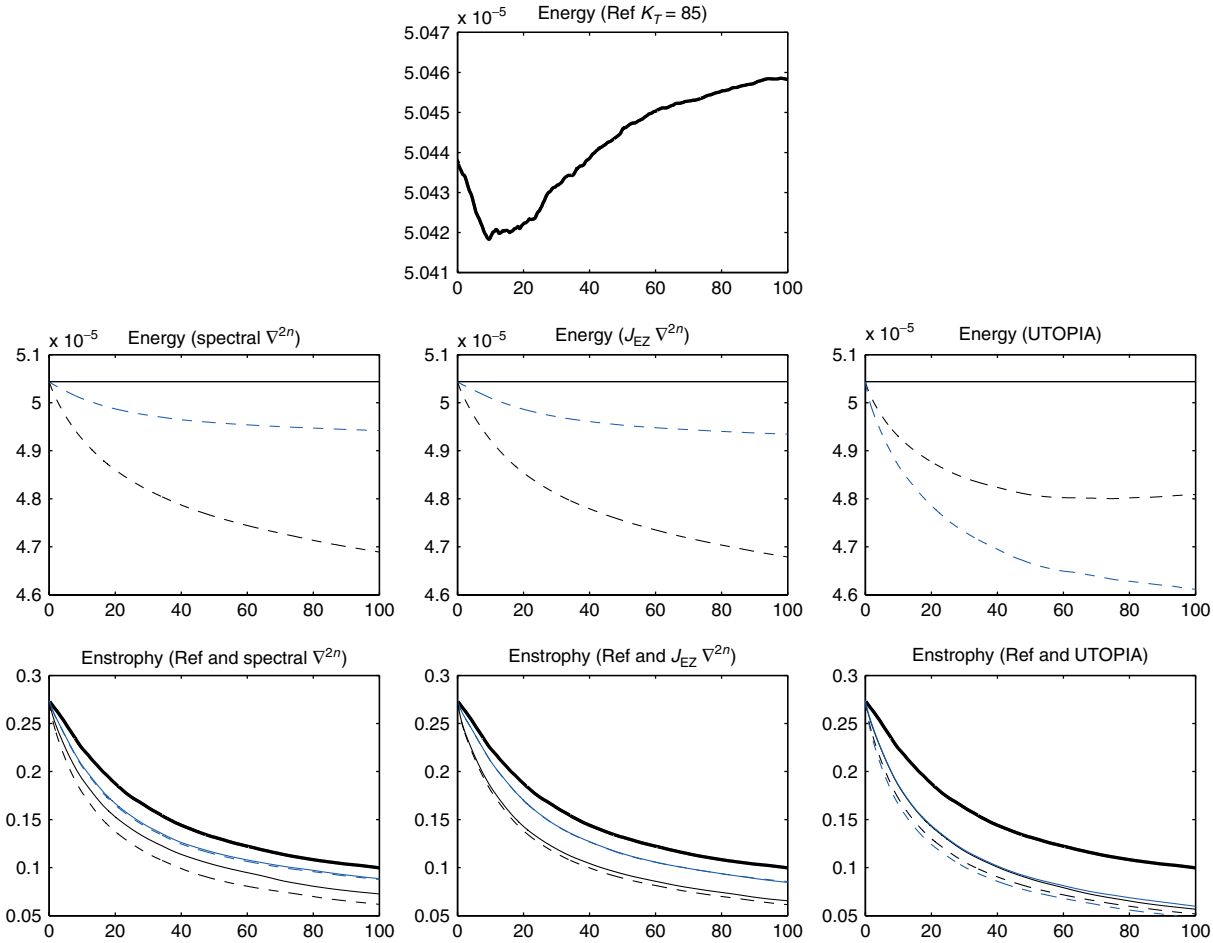

Figure 9. Energy and enstrophy time series for the freely decaying turbulence test. Top: energy at wave numbers $k < k_T = 85$ for the reference solution. Middle row: energy time series. Left: spectral ∇^4 (black, dashed), spectral ∇^4 plus fixer (black), spectral ∇^8 (blue, dashed), spectral ∇^8 plus backscatter (blue). Centre: J_{EZ} ∇^4 (black, dashed), J_{EZ} ∇^4 plus fixer (black), J_{EZ} ∇^8 (blue, dashed), J_{EZ} ∇^8 plus fixer (blue). Right: UTOPIA (black, dashed), UTOPIA plus fixer (black), UTOPIA with limiter (blue, dashed), UTOPIA with limiter plus fixer (blue). Bottom row: enstrophy time series; in all three panels the enstrophy for wave numbers $k < k_T = 85$ for the reference solution is shown as the heavy black line. Left: spectral ∇^4 (black, dashed), spectral ∇^4 plus fixer (black), spectral ∇^8 (blue, dashed), spectral ∇^8 plus backscatter (blue). Centre: J_{EZ} ∇^4 (black, dashed), J_{EZ} ∇^4 plus fixer (black), J_{EZ} ∇^8 (blue, dashed), J_{EZ} ∇^8 plus fixer (blue). Right: UTOPIA (black, dashed), UTOPIA plus fixer (black), UTOPIA with limiter (blue, dashed), UTOPIA with limiter plus fixer (blue).

impact on l_2 vorticity errors is marginal. For other schemes an intermediate-scale vorticity perturbation was found to be most effective. In this case the primary effect of the scheme is to repair the damage to the energy spectrum caused by truncation errors and excessive dissipation, and it leads to a modest reduction in l_2 vorticity errors. The scheme improves the long-term energy and enstrophy behaviour of the solution.

The results found here are suggestive of how to approach the problem in more complex equation sets and three-dimensional atmospheric models. Nevertheless, there are some caveats. As a practical matter, the evaluation of a suitable α (see Eq. (26)) will be less straightforward because the energy will no longer be a quadratic functional of the prognostic fields. At a more fundamental level, the dynamics may be sufficiently different to qualitatively alter the spectral transfers of energy and potential enstrophy: for three-dimensional compressible flow the influence of a potential vorticity anomaly on the balanced flow falls off exponentially with horizontal distance, rather than inversely with distance as it does in the barotropic vorticity equation; qualitatively different types of dynamics are possible, such as frontal formation or gravity wave generation and propagation; and there is significant forcing at small scales, e.g. from orography and convection. It would be valuable to extend the methodology described here to more complex and realistic flows to improve our understanding of the spectral transfers. Despite these caveats, given the results found here, it seems likely that schemes developed as backscatter models for weather and climate applications achieve their positive results, at least in part, by repairing damage to the energy spectrum caused by truncation errors and excessive dissipation rather than by modelling realistic backscatter.

Acknowledgements

We thank two anonymous reviewers for their constructive comments on an earlier version of this paper. This work was funded in part by Great Western Research and the Met Office.

References

Arakawa A. 1966. Computational design for long-term numerical integration of the equations of fluid motion: two-dimensional incompressible flow. Part I. *J. Comput. Phys.* **1**: 119–143.
Asselin R. 1972. Frequency filter for time integrations. *Mon. Weather Rev.* **100**: 487–490.
Batchelor GK. 1969. Computation of the energy spectrum in homogeneous two-dimensional turbulence. *Phys. Fluids* **12**: II–233.
Berner J, Shutts GJ, Leutbecher M, Palmer TN. 2009. A spectral stochastic kinetic energy backscatter scheme and its impact on flow-dependent predictability in the ECMWF ensemble prediction system. *J. Atmos. Sci.* **66**: 603–625.
Bowler NE, Arribas A, Beare SE, Mylne KR, Shutts GJ. 2009. The Local ETKF and SKEB: upgrades to the MOGREPS short-range ensemble prediction system. *Q. J. R. Meteorol. Soc.* **135**: 767–776.
Brown AR, MacVean MK, Mason PJ. 2000. The effects of numerical dissipation in large eddy simulations. *J. Atmos. Sci.* **57**: 3337–3348.
Chen S, Ecke RE, Eyink GL, Wang X, Xiao Z. 2003. Physical mechanism of the two-dimensional enstrophy cascade. *Phys. Rev. Lett.* **91**: 215401-1–215401-4.
Chen S, Ecke RE, Eyink GL, Wang X, Xiao Z. 2006. Physical mechanism of the two-dimensional inverse energy cascade. *Phys. Rev. Lett.* **96**: 084502-1–084502-4.
Domaradski JA, Saiki EM. 1997. Backscatter models for large-eddy simulations. *Theoret. Comput. Fluid Dynamics* **9**: 75–83.

Durran DR. 1999. *Numerical Methods for Wave Equations in Geophysical Fluid Dynamics*. Springer: Berlin.
Frederiksen JS, Kepert SM. 2006. Dynamical subgrid-scale parameterizations from direct numerical simulations. *J. Atmos. Sci.* **63**: 3006–3019.
Grinstein FF, Margolin LG, Rider W. 2007. *Implicit Large Eddy Simulation*. Cambridge University Press: Cambridge, UK.
Jablonowski C, Williamson DL. 2011. The pros and cons of diffusion, filters and fixers in atmospheric general circulation models. In *Numerical Techniques for Global Atmospheric Models*, Lauritzen PH, Jablonowski C, Taylor MA, Nair RD (eds). Springer: Berlin; 381–493.
Kent J, Thuburn J, Wood N. 2012. Assessing implicit large eddy simulation for two-dimensional flow. *Q. J. R. Meteorol. Soc.* **138**: 365–376.
Koshyk JN, Boer GJ. 1994. Parameterization of dynamical subgrid-scale processes in a spectral GCM. *J. Atmos. Sci.* **52**: 965–976.
Kraichnan RH. 1975. Statistical dynamics of two-dimensional flow. *J. Fluid Mech.* **67**: 155–175.
Kraichnan RH. 1976. Eddy viscosity in 2 and 3 dimensions. *J. Atmos. Sci.* **33**: 1521–1536.
Leonard BP, MacVean MK, Lock AP. 1993. Positivity-preserving numerical schemes for multidimensional advection. *NASA Technical Memorandum 106055*.
Lin SJ. 2004. A 'vertically Lagrangian' finite-volume dynamical core for global models. *Mon. Weather Rev.* **132**: 2293–2307.
Margolin LG, Rider WJ. 2002. A rationale for implicit turbulence modeling. *Int. J. Numer. Meth. Fluids* **39**: 821–841.
Margolin LG, Rider WJ. 2007. Numerical regularization: the numerical analysis of implicit subgrid models. In *Implicit Large-Eddy Simulation*, Grinstein FF, Margolin LG, Rider WJ (eds). Cambridge University Press: Cambridge, UK; 195–221.
Mason PJ, Thomson DJ. 1992. Stochastic backscatter in large-eddy simulations of boundary layers. *J. Fluid Mech.* **242**: 51–78.
Neale RB, Chen C-C, Gettelman A, Lauritzen PH, Park S, Williamson DL, Conley AJ, Garcia R, Kinnison D, Lamarque J-F, Marsh D, Mills M, Smith AK, Tilmes S, Vitt F, Cameron-Smith P, Collins WD, Iacono MJ, Rasch PJ, Taylor MA. 2010. Description of the NCAR Community Atmosphere Model (CAM 5.0). *NCAR Technical Note NCAR/TN-486+STR*.
Pietarila Graham J, Ringler T. 2013. A framework for the evaluation of turbulence closures used in mesoscale ocean large-eddy simulations. *Ocean Model.* (In press).
Rhines PB. 1979. Geostrophic turbulence. *Annu. Rev. Fluid Mech.* **11**: 401–441.
Robert A. 1966. The integration of a low order spectral form of the primitive meteorological equations. *J. Meteorol. Soc. Japan* **44**: 237–245.
Sadourny R, Basdevant C. 1985. Parameterization of subgrid scale barotropic and baroclinic eddies in quasi-geostrophic models: anticipated potential vorticity method. *J. Atmos. Sci.* **42**: 1353–1363.
Salmon R. 1998. *Lectures on Geophysical Fluid Dynamics*. Oxford University Press: Oxford.
Shutts G. 2005. A kinetic energy backscatter algorithm for use in ensemble prediction systems. *Q. J. R. Meteorol. Soc.* **131**: 3079–3102.
Smagorinsky J. 1963. General circulation experiments with the primitive equations. I. The basic experiment. *Mon. Weather. Rev.* **91**: 99–164.
Thuburn J. 1996. Multidimensional flux-limited advection schemes. *J. Comput. Phys.* **123**: 74–83.
Thuburn J. 2008. Some conservation issues for the dynamical cores of NWP and climate models. *J. Comput. Phys.* **227**: 3715–3730.
Williamson DL. 2007. The evolution of dynamical cores for global atmospheric models. *J. Meteorol. Soc. Japan* **85B**: 241–269.
Williamson DL, Olson JG, Jablonowski J. 2009. Two dynamical core formulation flaws exposed by a baroclinic instability test case. *Mon. Weather Rev.* **137**: 790–796.
WGNE. 2003. WMO Atmospheric Research and Environment Programme. Report No. 18, CAS/JSC Working Group on Numerical Experimentation.